ACS Energy LETTERS

http://pubs.acs.org/journal/aelccp

High-Pressure Electrochemical CO_2 Capture and Reduction to Formic Acid

Wei Ping Lam, Tae-Ung Wi, Ahmad Elgazzar, Shaoyun Hao, Malik Paulino, Valery Okatenko, Chase Sellers, Junwei Zhang, and Haotian Wang*

Cite This: *ACS Energy Lett.* 2025, 10, 5466−5473

Read Online

ACCESS | Metrics & More | Article Recommendations | Supporting Information

ABSTRACT: **Direct supply of dilute CO_2 sources to an electrochemical porous solid electrolyte (PSE) reactor enables simultaneous CO_2 capture and conversion. However, its catalytic performance is significantly limited under ambient pressure due to low CO_2 surface coverage and mass transport constraints. Here, we demonstrate a high-pressure CO_2 reduction reaction (CO_2RR) of a dilute stream in a PSE reactor, achieving markedly enhanced formic acid selectivity. Pressurizing a 5 mol % CO_2 gas stream to 10 atm led to a Faradaic efficiency for formic acid (FE_{HCOOH}) of up to 81.0% at 100 mA cm^{-2}, compared to only 47.8% under ambient conditions. By balancing the liquid pressure within the PSE layer with the cathode gas pressure, we minimized the transmembrane pressure differential, enabling stable operation for 90 h at 20 atm. In addition, high-pressure operation shifted the cathode-membrane interfacial pH from a carbonate-dominated regime toward bicarbonate, thereby improving the electron efficiency of the simultaneous carbon capture process by up to 57.0% during the conversion process.**

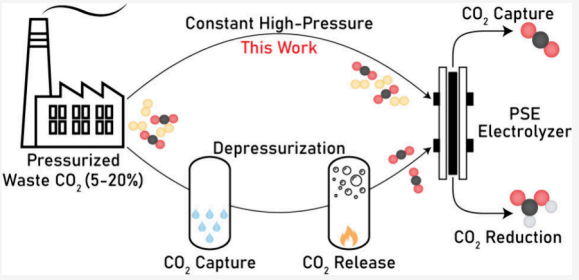

Practical strategies to capture and utilize carbon dioxide (CO_2) from low-concentration sources, including ambient air and industrial tail/flue gases, are increasingly important in the context of sustainable chemical synthesis and robust manufacturing chains.[1] The electrochemical reduction of CO_2 into valuable chemicals (such as formic acid) represents a promising approach for CO_2 utilization integrated with renewable energy.[2,3] But traditional electrochemical CO_2 reduction reaction (CO_2RR) electrolyzers face significant challenges when adjusted to dilute CO_2 streams, including low catalytic activity and selectivity due to limited reactant mass transport.[4−6] Consequently, in an industrial setting, these methods would require costly CO_2 purification steps and may incur a depressurization penalty before electrolysis when sourcing carbon from flue gas or directly from air. In response, we leverage dilute-CO_2 point sources already pressurized enough to achieve sufficient CO_2 mass transport for high activity.[7,8] Mainly, the tail gas of steam methane reforming (SMR) and subsequent water-gas shift reaction for blue hydrogen production may comprise 9−20 mol % CO_2 pressurized around 15−30 atm.[9,10] Advantageously, point-source CO_2 conversion bypasses the conventional multistep approach for carbon utilization and could achieve a higher energy efficiency and cost savings for the whole process. Although nascent in the literature, the impact of trace impurities in tail gases, such as NO_x and SO_x, on electrochemical CO_2RR has shown optimistic results, specifically, that bismuth-based catalysts without modification for formate production can tolerate NO and SO_2 impurities.[11] However, technical challenges, such as effects of oxygen content and electrolyzer reliability under high pressure, persist, and extensive efforts need to be made in our field.[4]

Currently, most CO_2RR studies operate at atmospheric pressures with high-purity CO_2 gas as the feedstock, but these idealized conditions may not be viable for industry-scale electrolysis. As the field advances to larger scales, electrolyzers may need to adopt high-pressure systems to maintain high efficiencies and manage considerable pressure drops in gas flow fields.[12−15] Many preliminary studies focused on high-pressure conditions were only done with aqueous electrolyzers. In some cases, researchers linked the improved CO_2RR Faradaic efficiency (FE) to increased solubility of dissolved CO_2 in electrolytes.[16−20] In other cases, high liquid pressures influenced the reaction environment to cause a change in product selectivity.[21−23] Still, membrane electrode assembly (MEA)-based electrolysis with the development of the gas diffusion electrode (GDE) is more practical for delivering

Received: July 11, 2025
Revised: September 5, 2025
Accepted: September 9, 2025
Published: October 14, 2025

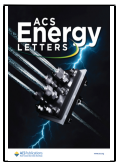

https://doi.org/10.1021/acsenergylett.5c02165
ACS Energy Lett. 2025, 10, 5466−5473

industrial-relevant current densities.[24] The use of higher gas pressures in MEAs has shown improved electrocatalytic performance due to increased CO_2 coverage on the catalytic surface.[25−28] Therefore, we sought to develop an advanced high-pressure electrolyzer with a low-concentration of CO_2 as a feedstock.

Previously, we established using a porous solid electrolyte (PSE) reactor for several electrochemical applications, including high-purity formic acid synthesis and CO_2 capture from simulated flue gas.[29−35] Compared with conventional MEA reactors with two chambers, our reactor contains a third PSE interlayer to exploit ionic movement. Here, in this study, to evaluate the potential of using our PSE reactor under high-pressure operation, we demonstrated a simultaneous reduction and capture of low-concentration CO_2 with a PSE reactor. This method presents an attractive route for formic acid production as we avoid the carbon capture step by directly feeding a low-concentration, high-pressure source, as well as the separation costs of formate from liquid electrolytes used in conventional CO_2 electrolyzers (Figure 1). At the same time, the extra PSE

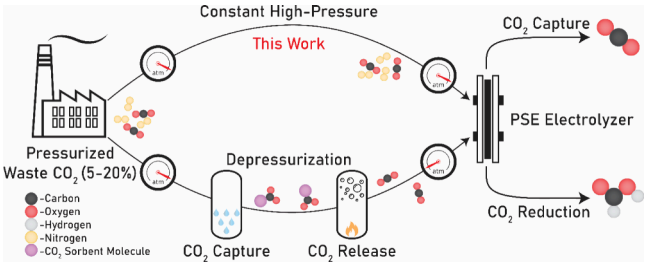

Figure 1. Process overview of waste CO_2 utilization. This work focuses on maintaining and utilizing the high-pressure of waste CO_2 (for example, steam methane reforming tail gas) to do the CO_2RR, while typical studies rely on the purification of waste CO_2, which involves an energy intensive capture and release process with a depressurization penalty, before electrolysis. The high pressure of low-concentration CO_2RR has electrochemical activity similar to that of pure CO_2 at atmospheric conditions, presenting this work as a robust and simplified pathway. We further extend this study by utilizing a PSE electrolyzer architecture. The PSE electrolyzer adds value by simultaneously capturing CO_2 (in the case of low-concentration CO_2 feed) or recovering lost CO_2 (with pure CO_2 feeds) while electrochemically reducing CO_2 to high-purity formic acid.

layer helps to mitigate the significant carbon loss issue (which could be even more prominent under high-pressure operations) inherent to alkaline-based MEA CO_2 electrolysis.[36] Instead, CO_2 is continuously recovered as a high-purity stream from the solid-electrolyte middle chamber.[33]

In this study, with 10 mol % CO_2, we successfully demonstrated a 91.2% FE toward formic acid (FE_{HCOOH}) at 100 mA cm^{-2} and 91.1% FE_{HCOOH} at 150 mA cm^{-2} by increasing the pressure to 5 atm. Utilizing 5 mol % CO_2 also shows significant improvement from 47.5% FE_{HCOOH} at 1 atm to 81.0% FE_{HCOOH} at 10 atm at 100 mA cm^{-2}. The high pressures also boosted carbon capture rates up by 57.0% (relative, for 1−7.5 atm, from 0.204 to 0.320 mL min^{-1} cm^{-2}) for 10 mol % CO_2 and 18.1% (relative, for 1−5 atm, from 0.218 to 0.258 mL min^{-1} cm^{-2}) for 5 mol % CO_2 at 100 mA cm^{-2}. In recent years, a handful of studies have reported low-concentration CO_2RR (5−15 mol %) via microenvironment tuning and CO_2 enrichment strategies, but these are still limited by short stability under 30 h and versatility.[7,37−42] Therefore, we showed 90 h stability with >70% FE_{HCOOH} at 50 mA cm^{-2} using 5 mol % CO_2 at 20 atm. This high-pressure approach can be a broad tool to convert low-concentration CO_2 for various catalysts and electrochemical cell configurations.

We adapted our original PSE reactor to accommodate high pressures with a few modifications (Figure 2a, Supporting

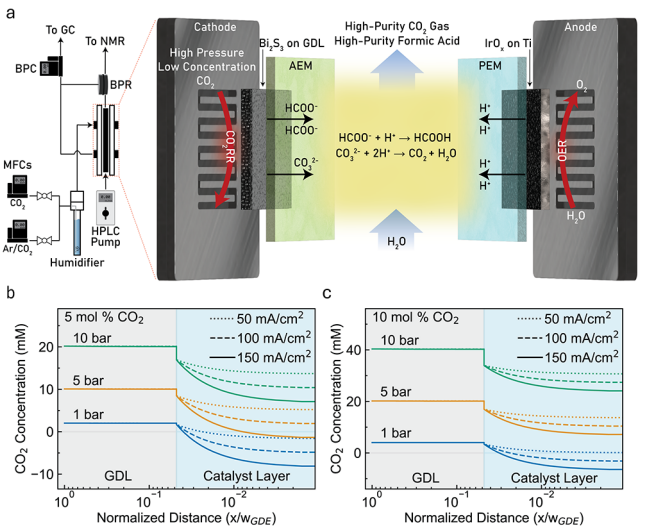

Figure 2. High-pressure diagram and mechanisms of low-concentration CO_2RR and capture. (a) High-pressure equipment setup and expanded view of the PSE reactor illustrating the simultaneous CO_2 capture and conversion concept. BPC: back-pressure controller. BPR: back-pressure regulator. MFC: mass flow controller. GC: gas chromatography. NMR: nuclear magnetic resonance. HPLC: high-performance liquid chromatography. COMSOL Multiphysics simulations of steady-state CO_2 concentration in the GDE of (b) 5 mol % and (c) 10 mol % CO_2 at different pressures. CO_2 is consumed at the catalyst-membrane interface, assuming a 100% FE toward reducing CO_2 at each current density. Negative CO_2 concentrations denote complete consumption of CO_2 and do not have significant meaning other than HER must be occurring to sustain the current density.

Information Figure S1). First, we replaced standard polytetrafluoroethylene (PTFE) gaskets that hold the GDEs in place with a silicon material to create a gastight seal within the cell. Next, we replaced all nylon and polypropylene fittings with stainless-steel Swagelok compression fittings and vinyl tubing with either PTFE, copper, or polyether ether ketone (PEEK) material to prevent leaks between different equipment (Supporting Information Figure S2). A custom-made stainless-steel piece was utilized to bubble gas through deionized water for humidifying gas at high pressures. Lastly, we replaced the peristaltic pump with an HPLC-grade piston pump to flow deionized (DI) water or 3 mM $KHCO_3$ into the middle chamber and added a gas back-pressure controller (BPC) and liquid back-pressure regulator (BPR), all built to withstand up to 34 atm. Due to the anion exchange membrane's (AEM) inadequate mechanical strength and the PSE being loose-standing particles (and therefore pliable), too much stress from the cathode-side pressure could tear the AEM. So we designed the system to have a minimal pressure differential across the AEM by using the gas pressure to push a diaphragm in the BPR that regulates the liquid pressure. In contrast, the

https://doi.org/10.1021/acsenergylett.5c02165
ACS Energy Lett. 2025, 10, 5466−5473

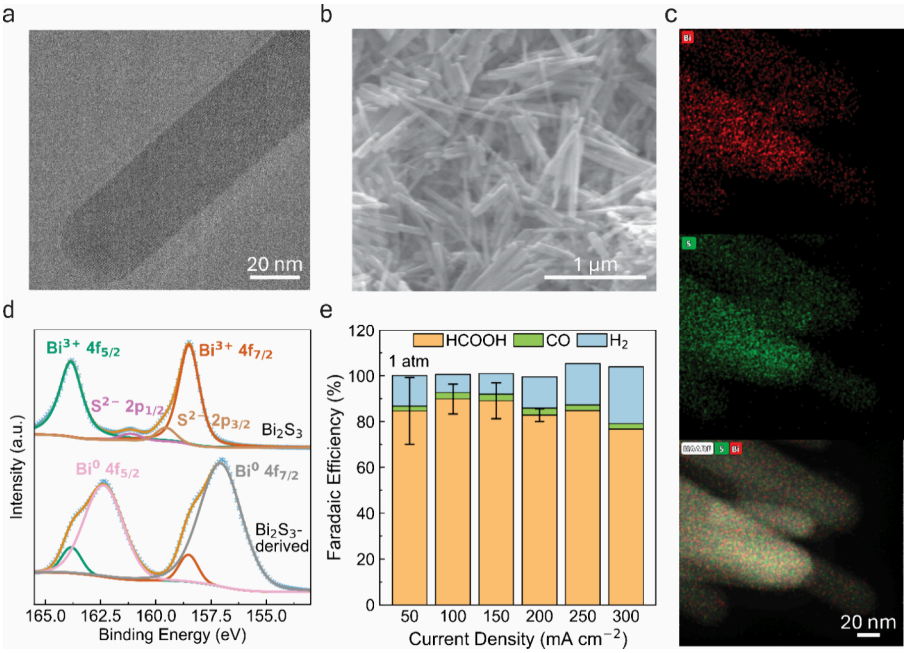

Figure 3. Characterization of prereduced Bi_2S_3 catalyst and performance. (a) TEM image, (b) SEM image, (c) HAADF-STEM with EDS elemental mapping of Bi and S of Bi_2S_3 catalyst. (d) XPS narrow scan of (top) pre- and (bottom) postreduction Bi_2S_3 catalyst. (e) Electrochemical CO_2RR FE in a nonpressurized PSE reactor with pure CO_2 feed. Average values from three independent tests are shown with error bars (FE_{HCOOH} only) representing one standard deviation for current densities of 50−200 mA cm^{-2}. Otherwise, average values from two independent tests are shown.

excellent mechanical strength of the proton exchange membrane (PEM) allows the anode reaction to occur at ambient pressure. Therefore, we could use a low pressure-rated peristaltic pump to flow DI water on the anode. This aspect of the PSE reactor allows us to decouple the cathode and anode operating pressures which may be beneficial for certain redox reactions, whereas some AEM-based MEAs may not be able to.

The chemistry within the electrolyzer is straightforward: the electrochemical CO_2RR into formate in an alkaline environment releases free hydroxide ions that chemically react with excess CO_2 to form (bi)carbonates at the high alkaline interface. In a PSE reactor design, formate and carbonate anions co-transport through an AEM and are neutralized to release pure CO_2 in the gas phase and high-purity formic acid in the liquid phase (Figure 2a). The anions are neutralized by running an acidic oxygen evolution reaction (OER) on the anode side, allowing generated protons to migrate through a PEM.

According to COMSOL Multiphysics simulations, the high-pressure operation shows an increase in the CO_2 concentration in the catalyst layer (Figure 2b,c and Supporting Information Note 1). For both 5 and 10 mol % CO_2, there is not enough CO_2 available at the reaction interface to achieve high CO_2RR performance when operating at 1 bar. However, at 5 and 10 bar, there is theoretically enough CO_2 to achieve 100% CO_2RR FE (except at 150 mA cm^{-2} where greater than 5 bar is needed to fully convert 5 mol % CO_2) showcasing that elevating the pressure can have a significant impact on electrochemical activity.

To demonstrate low-concentration CO_2RR, we sought a well-defined electrocatalyst for formic acid production under standard conditions. Adopted from previous literature, we synthesized Bi_2S_3 nanorods via hydrothermal method due to its facile synthesis process and high CO_2RR performance.[43] The transmission electron microscopy (TEM) and scanning electron microscopy (SEM) images of the as-obtained Bi_2S_3 catalyst confirm its nanorod-like structure that is consistent with the literature (Figure 3a,b and Supporting Information Figure S3). Energy-dispersive X-ray spectroscopy (EDS) element maps show uniformly distributed Bi and S elements within the catalyst at approximately a 41.1:58.9 atomic ratio (Figure 3c and Supporting Information Figure S5). X-ray diffraction (XRD) results clearly show that the catalyst follows the facet structure of Bi_2S_3 (Supporting Information Figure S6). We directly applied this electrocatalyst to our PSE reactor system under regular CO_2RR electrolysis conditions (100 mol % CO_2, ambient pressure) to verify its intrinsic activity (Figure 3e and Supporting Information Figure S10). We obtained 89.9% FE_{HCOOH} at 100 mA cm^{-2} at a full cell voltage of 3.40 V, which suggests impressive formic acid selectivity/activity and is consistent with our previous reports of bismuth-based catalysts in PSE reactors.[29−32] Proton ^1H NMR and ion chromatography (IC) results show that formic acid is of high-purity demonstrating the PSE reactor's ability to produce pure liquid fuels (Supporting Information Figures S8 and S9). Since postreaction SEM images showed an agglomerated morphology and the Bi_2S_3 catalyst turned from dark gray to black color after catalysis, we hypothesized that it could undergo a prereduction to metallic phase as we typically see with many metal sulfide and oxide catalysts in cathodic reactions (Supporting Information Figure S4).[43−47] To verify this, we performed postelectrolysis XRD with sophisticated experimental steps to avoid catalyst reoxidation (Supporting Information Methods). The result shows that the catalyst was reduced to Bi^0 after the preactivation process under CO_2RR (Supporting Information Figure S6). In agreement with XRD, postelectrolysis X-ray photoelectron spectroscopy (XPS) also shows the removal of sulfur and formation of

https://doi.org/10.1021/acsenergylett.5c02165
ACS Energy Lett. 2025, 10, 5466−5473

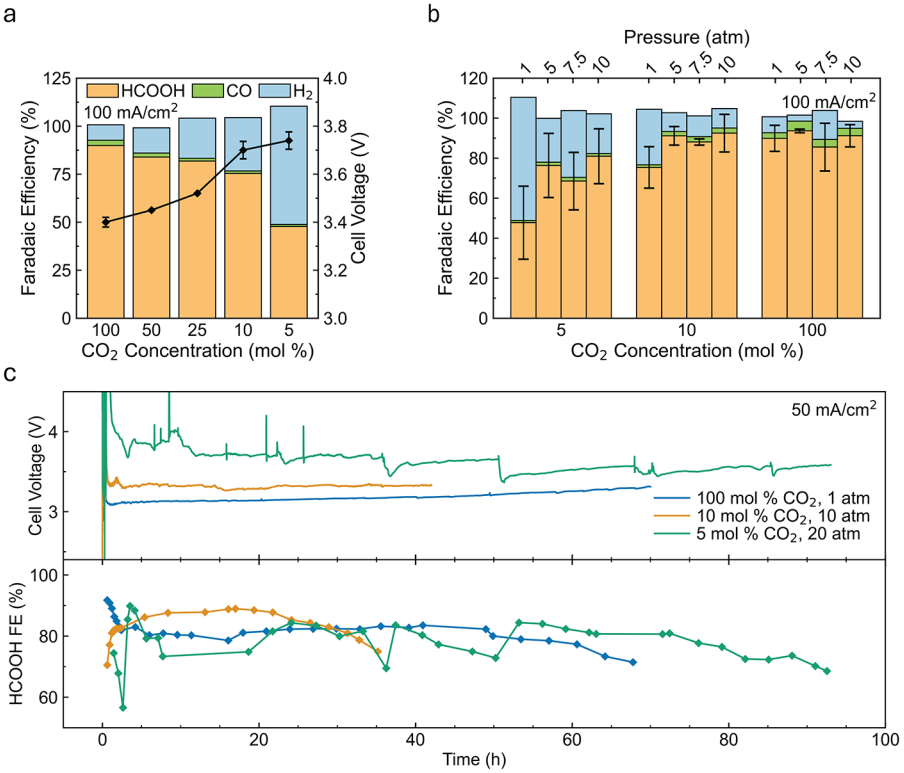

Figure 4. Electrochemical CO_2RR performance with a PSE reactor. (a) CO_2RR Faradaic efficiency and corresponding cell voltage at different CO_2 concentrations under ambient temperature and (b) with increasing pressure at 100 mA cm^{-2}. (c) Long-term stability test of the CO_2RR at different CO_2 concentrations and pressures at 50 mA cm^{-2} showing (top) voltages and (bottom) FE_{HCOOH}'s calculated by 100 minus the FE of hydrogen and CO due to frequent and automated collection of gas chromatography data. Average values of (a) voltages of 5, 10, and 100 mol % CO_2 and (b) FE_{HCOOH}'s from three independent tests are shown with error bars representing one standard deviation.

metallic bismuth due to electroreduction (Figure 3d and Supporting Information Figure S7).

We presume that the main challenge in low-concentration CO_2 is its sluggish mass transfer to the electrocatalytically active sites. Maintaining the current density at 100 mA cm^{-2}, we gradually decreased the CO_2 concentration to see its impact on FE_{HCOOH} and cell voltage under ambient pressure (Figure 4a). Notable differences in performance are seen once the CO_2 concentration reaches below 25 mol %, at which voltages start to increase above 3.70 V and the hydrogen evolution reaction (HER) becomes more prominent. At 50 mA cm^{-2}, although a change in FE is less noticeable, the voltage still increased 250 mV, meaning that even under lower current densities and CO_2 consumption rates, there might still be some conversion inefficiency since we are nearly choking the GDE of CO_2 (Supporting Information Figures S11 and S13). At 150 mA cm^{-2}, the FE change became more dramatic as the CO_2RR became limited by the mass diffusion of CO_2 to the catalyst surface compared to the reaction rate. These results agree with COMSOL simulations that at 100 and 150 mA cm^{-2}, where CO_2 availability is limiting and we cannot obtain high FE_{HCOOH}. Also, at 50 mA cm^{-2}, there is scarcely enough CO_2 to achieve a moderate performance.

To recover the CO_2RR FE losses, we elevated the gas stream pressure to ensure sufficient CO_2 coverage on the catalyst (Figure 4b). In the case of 10 mol % CO_2, at 100 mA cm^{-2}, increasing the total absolute pressure to 5 atm brings the FE_{HCOOH} from 75.4% back up to 91.2%, mimicking the formic acid production rate (~1.70 mmol h^{-1} cm^{-2}) of pure CO_2RR at atmospheric pressure. For 5 mol % CO_2, the FE_{HCOOH} is not fully recovered, but there remains a significant improvement in the FE_{HCOOH} from 47.8% to 76.4% at 5 atm and even to 81.0% at 10 atm. A similar phenomenon was observed with 5 and 10 mol % CO_2 when maintaining the current density at 150 mA cm^{-2}, where there is a clear increase in FE_{HCOOH} at elevated pressures (Supporting Information Figure S14). These results indicate that high pressures significantly improve CO_2 mass transport to the catalyst layer such that we obtain great formic acid selectivity and activity at such low CO_2 feed concentrations.

Overall, for pure CO_2, the voltages remain relatively constant at any pressure (Supporting Information Figure S12). In contrast, for 10 mol % CO_2, the voltage decreases 180 mV from 1 to 7.5 atm, likely due to decreasing HER and, thus, a lower overpotential to drive the Faradaic current on the bismuth-based catalyst. However, further increasing the pressure to 10 atm caused a notable increase in the voltage. This may be due to the presence of argon, which at high pressures could become unsupportive to ionic conduction. Another possibility is that the high pressures induce GDE and AEM delamination during the reaction, which could also adversely affect ionic conduction. For 5 mol % CO_2, the voltages remain higher, presumably from inefficient HER and high argon flow. These results suggest that challenges remain in energy efficiency for low-concentration CO_2RR due to inflated voltages.

We then performed stability tests for the different CO_2 concentrations where the partial pressure of CO_2 remained near 1 atm at 50 mA cm^{-2} (Figure 4c and Supporting Information Figure S15). The stability of the tests ranged from

https://doi.org/10.1021/acsenergylett.5c02165
ACS Energy Lett. 2025, 10, 5466−5473

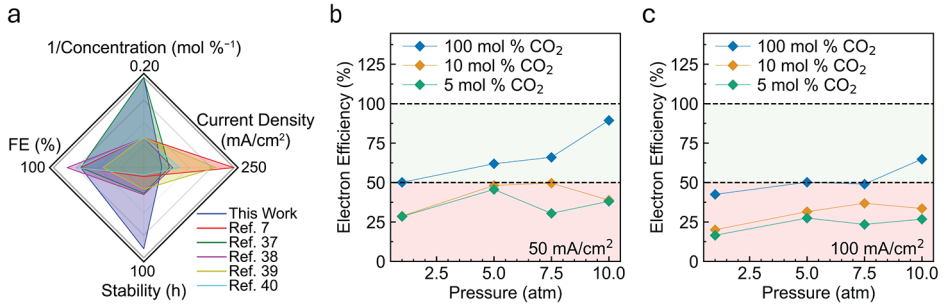

Figure 5. Electrochemical performance metrics and carbon capture efficiency with a PSE reactor. (a) This work's catalytic performance compared to other low-concentration CO_2RR works reported in literature. Carbon capture electron efficiencies for different pressures at (b) 50 mA cm^{-2} and (c) 100 mA cm^{-2}. The electron efficiency is calculated as discussed in Supporting Information Note 2. The bottom red region represents CO_2 from carbonate crossover, and the top green region represents a combination of carbonate and bicarbonate crossover.

42 to 90 h, during which the FE_{HCOOH} remained above 70% (correlating to greater than 0.65 mmol h^{-1} cm^{-2} of formic acid), proving the robustness of high-pressure as a method to convert low concentrations of CO_2. The variability in stability time may be caused by the difference in total gas flow rates that could result in varying rates of gas diffusion layer (GDL) flooding. It could also be due to small differences in interlayer contact arising from variations in cell assembly, which may become more pronounced under high-pressure operation.[48] We ruled out the catalyst as a factor in degradation since, with pure CO_2 at 5 atm, we could maintain >90% FE_{HCOOH} at 100 mA cm^{-2} for at least 338 h, suggesting that GDL flooding was the limiting factor (Supporting Information Figure S16). Nonetheless, this work's stability exceeds that of other studies involving low-concentration CO_2RR (Figure 5a and Supporting Information Table S3). We maintained high FE while pushing lower CO_2 concentrations; however, this is in part due to running a lower current density. But, anyone at a current density higher than 100 mA cm^{-2} uses CO_2 with a concentration three times greater (15 mol % CO_2) which creates a skewed comparison but highlights the limited research of low-concentration CO_2RR.

In the CO_2RR, high pressure may also influence the local reaction environment at the catalyst-membrane interface. The alkaline CO_2RR produces hydroxide ions (OH^-) creating a basic environment (eq 1). CO_2 rapidly buffers the interface by chemically reacting with OH^- to form carbonate species that will crossover the AEM (eqs 2 and 3).[36] For every 2 mol of electrons transferred for CO_2RR to formate, 1 mol of CO_2 can be captured as bicarbonate (eq 2) and neutralized in the middle chamber, which we assume to be 100% electron efficiency since electrons (or produced hydroxides) are utilized fully toward achieving the maximum theoretical carbon capture rate. In the case of carbonate species formation (eq 3), only 0.5 mol of CO_2 can be captured, which we assume to be 50% electron efficiency.

$$CO_2 + 2e^- + H_2O \rightarrow HCOO^- + OH^- \quad (1)$$

$$CO_2 + OH^- \rightarrow HCO_3^- \quad (2)$$

$$\frac{1}{2}CO_2 + OH^- \rightarrow \frac{1}{2}CO_3^{2-} + \frac{1}{2}H_2O \quad (3)$$

At atmospheric pressure, we typically observed only the crossover of carbonate ions. But at higher pressures, with higher availability of CO_2 at the interface, there may be a slight decrease in pH from the acidity of CO_2. This pH change could partially push the carbonaceous species in solution from carbonate to bicarbonate at the interface. This could be why we can produce stable results at 50 mA cm^{-2} when the partial pressure of CO_2 is 1 atm, since we may slightly produce bicarbonate at the interface rather than inside the GDL, partially preventing flooding (Figure 5b). Moreover, at 100 mA cm^{-2}, when the pressure is 1 atm, we practically see only carbonate crossover (Figure 5c). However, at 5 atm, for pure CO_2, the interfacial anions include some bicarbonate and we obtain improved stability. Although we observe better stability when bicarbonate ions are formed, more evidence is required to show that direct bicarbonate formation helps prevent flooding or supports better conduction.

With the help of elevated pressure, carbon capture rates tend to increase. At 100 mA cm^{-2}, the carbon capture increases a relative 57.0% from 1 to 7.5 atm for 10 mol % CO_2 and a relative 18.1% from 1 to 5 atm for 5 mol % CO_2 (Supporting Information Figure S18). However, these carbon capture rates are not normalized to the FE since electrosynthesis of hydrogen and CO produces two hydroxides, resulting in higher theoretical capture rates than OH^- produced with formic acid. Therefore, the carbon capture results may better be represented by the electron efficiency, which is normalized to the FE. Generally, as the pressure increases from 1 to 5 atm, the electron efficiency increases because of increased CO_2 activity (Figure 5b,c and Supporting Information Figure S17). At 7.5 and 10 atm, there seem to be some abnormalities with the electron efficiency of 5 and 10 mol % CO_2; however, the measured carbon capture rates fall within error (Supporting Information Figure S18). Regardless, at 50 mA cm^{-2}, we reach a peak electron efficiency of 49.6% (a 72.7% relative increase from 1 atm), and 36.9% (an 83.5% relative increase from 1 atm) at 100 mA cm^{-2} for capturing 10 mol % CO_2. Similarly, for 5 mol % CO_2, we can achieve up to a 65.6% relative increase in electron efficiency. This data show that we obtain greater electron efficiencies at the expense of some pressure, resulting in a possible synergistic effect with stability.

We demonstrated the PSE reactor's capability to operate at high pressures of up to 20 atm. The high pressures function to increase the CO_2 concentration, which boosts the CO_2 activity at the catalyst-membrane interface for electrochemical CO_2RR and CO_2 capture purposes. With this, we directly convert low concentrations of CO_2 into valuable liquid products at high efficiencies with stability for up to 90 h. Simultaneously, we capture CO_2 at greater rates via (bi)carbonate formation and crossover at the alkaline interface. This work could be extended to other catalysts of interest for the electrosynthesis of other liquid fuels (such as ethanol) from CO_2, as this is a

https://doi.org/10.1021/acsenergylett.5c02165
ACS Energy Lett. 2025, 10, 5466−5473

catalyst-independent method. For future work, it may be possible to leverage the PSE reactor's ability to run high-pressure hydrogen oxidation reaction (HOR) on the anode side, further integrating this system within an SMR process.[29,30,35,49]

■ ASSOCIATED CONTENT

Supporting Information

The Supporting Information is available free of charge at https://pubs.acs.org/doi/10.1021/acsenergylett.5c02165.

Experimental methods, COMSOL model parameters, CO_2 capture electron efficiency calculation, photographs of PSE reactor and high-pressure setup, SEM images, EDX spectrum, XPS and XRD characterization, ^1H NMR spectrum, IC chromatogram, supporting electrochemical CO_2RR performance, supporting carbon capture performance, and comparison table of low-concentration CO_2RR works (PDF)

■ AUTHOR INFORMATION

Corresponding Author

Haotian Wang − *Department of Chemical and Biomolecular Engineering, Rice University, Houston, Texas 77005, United States; Department of Chemistry, Department of Materials Science and NanoEngineering, Rice Advanced Material Institute, and Rice WaTER Institute, Rice University, Houston, Texas 77005, United States;* orcid.org/0000-0002-3552-8978; Email: htwang@rice.edu

Authors

Wei Ping Lam − *Department of Chemical and Biomolecular Engineering, Rice University, Houston, Texas 77005, United States;* orcid.org/0000-0002-0458-4520

Tae-Ung Wi − *Department of Chemical and Biomolecular Engineering, Rice University, Houston, Texas 77005, United States;* orcid.org/0000-0002-8295-825X

Ahmad Elgazzar − *Department of Chemical and Biomolecular Engineering, Rice University, Houston, Texas 77005, United States;* orcid.org/0000-0003-1453-4938

Shaoyun Hao − *Department of Chemical and Biomolecular Engineering, Rice University, Houston, Texas 77005, United States;* orcid.org/0000-0001-8353-518X

Malik Paulino − *Department of Chemical and Biomolecular Engineering, Rice University, Houston, Texas 77005, United States*

Valery Okatenko − *Department of Chemical and Biomolecular Engineering, Rice University, Houston, Texas 77005, United States;* orcid.org/0000-0002-7542-7995

Chase Sellers − *Department of Chemical and Biomolecular Engineering, Rice University, Houston, Texas 77005, United States*

Junwei Zhang − *Department of Chemical and Biomolecular Engineering, Rice University, Houston, Texas 77005, United States*

Complete contact information is available at: https://pubs.acs.org/10.1021/acsenergylett.5c02165

Author Contributions

W.P.L., T.-U.W., and H.W. conceptualized the project. W.P.L. prepared and performed all electrochemical experiments and analyzed data. W.P.L. collected TEM, STEM-HAADF, and EDS images. A.E. performed COMSOL simulation. S.H. gathered SEM images and XRD data. M.P. synthesized the Bi_2S_3 catalyst. V.O. and S.H. assisted in designing figures and schematics. C.S. collected XPS data. J.Z. helped to maintain and tend to some stability tests and tested IC samples. W.P.L. and H.W. wrote the paper. W.P.L., T.-U.W., A.E., V.O., and H.W. discussed experimental data.

Notes

The authors declare no competing financial interest.

■ ACKNOWLEDGMENTS

This work was supported by Rice University, the Department of Energy (Grant DE-EE00010839), the Robert A. Welch Foundation (Grant C-2051-20230405), and Sandia National Laboratories (Grant SNL-2532992). Analytical instruments used for characterization were provided by the Shared Equipment Authority (SEA) at Rice University.

■ REFERENCES

(1) Kazemifar, F. A Review of Technologies for Carbon Capture, Sequestration, and Utilization: Cost, Capacity, and Technology Readiness. *Greenh. Gases Sci. Technol.* **2022**, *12* (1), 200−230.

(2) Nankya, R.; Elgazzar, A.; Zhu, P.; Chen, F.-Y.; Wang, H. Catalyst Design and Reactor Engineering for Electrochemical CO2 Reduction to Formate and Formic Acid. *Mater. Today* **2024**, *76*, 94−109.

(3) Bushuyev, O. S.; De Luna, P.; Dinh, C. T.; Tao, L.; Saur, G.; van de Lagemaat, J.; Kelley, S. O.; Sargent, E. H. What Should We Make with CO2 and How Can We Make It? *Joule* **2018**, *2* (5), 825−832.

(4) O'Brien, C. P.; Miao, R. K.; Shayesteh Zeraati, A.; Lee, G.; Sargent, E. H.; Sinton, D. CO2 Electrolyzers. *Chem. Rev.* **2024**, *124* (7), 3648−3693.

(5) Kim, D.; Choi, W.; Lee, H. W.; Lee, S. Y.; Choi, Y.; Lee, D. K.; Kim, W.; Na, J.; Lee, U.; Hwang, Y. J.; Won, D. H. Electrocatalytic Reduction of Low Concentrations of CO2 Gas in a Membrane Electrode Assembly Electrolyzer. *ACS Energy Lett.* **2021**, *6* (10), 3488−3495.

(6) Kim, B.; Ma, S.; Molly Jhong, H.-R.; Kenis, P. J. A. Influence of Dilute Feed and pH on Electrochemical Reduction of CO2 to CO on Ag in a Continuous Flow Electrolyzer. *Electrochim. Acta* **2015**, *166*, 271−276.

(7) Xu, Y.; Edwards, J. P.; Zhong, J.; O'Brien, C. P.; Gabardo, C. M.; McCallum, C.; Li, J.; Dinh, C.-T.; Sargent, E. H.; Sinton, D. Oxygen-Tolerant Electroproduction of C2 Products from Simulated Flue Gas. *Energy Environ. Sci.* **2020**, *13* (2), 554−561.

(8) Li, Y.; Liu, H.; Raj, J.; Pishnamazi, M.; Wu, J. Elevated Temperature and Pressure Driven Ampere-Level CO 2 Electroreduction to CO in a Membrane Electrode Assembly Electrolyzer. *EES Catal.* **2025**, *3*, 843−855.

(9) Slivka, R. M.; Chinn, M. S.; Grunden, A. M. Gasification and Synthesis Gas Fermentation: An Alternative Route to Biofuel Production. *Biofuels* **2011**, *2* (4), 405−419.

(10) García, L. 4- Hydrogen Production by Steam Reforming of Natural Gas and Other Nonrenewable Feedstocks. In *Compendium of Hydrogen Energy*; Subramani, V., Basile, A., Veziroğlu, T. N., Eds.; Woodhead Publishing Series in Energy; Woodhead Publishing: Oxford, 2015; pp 83−107, DOI: 10.1016/B978-1-78242-361-4.00004-2.

(11) Van Daele, S.; Hintjens, L.; Hoekx, S.; Bohlen, B.; Neukermans, S.; Daems, N.; Hereijgers, J.; Breugelmans, T. How Flue Gas Impurities Affect the Electrochemical Reduction of CO2 to CO and Formate. *Appl. Catal. B Environ.* **2024**, *341*, 123345.

(12) Crandall, B. S.; Ko, B. H.; Overa, S.; Cherniack, L.; Lee, A.; Minnie, I.; Jiao, F. Kilowatt-Scale Tandem CO2 Electrolysis for Enhanced Acetate and Ethylene Production. *Nat. Chem. Eng.* **2024**, *1*, 421−429.

(13) Kani, N. C.; Olusegun, S.; Chauhan, R.; Gauthier, J. A.; Singh, M. R. High-Pressure Electrochemistry: A New Frontier in Decarbonization. *EES Catal.* **2024**, *2*, 507−521.

(14) Li, Y.; Shao, G.; Zheng, X.; Jia, Y.; Xia, Y.; Dou, Y.; Huang, M.; Gu, C.; Shi, J.; Zheng, J.; Dou, S. Cutting-Edge Advances in Pressurized Electrocatalytic Reactors. *eScience* **2025**, *5*, 100369.
(15) Fink, A. G.; Navarro-Pardo, F.; Tavares, J. R.; Legrand, U. Scale-up of Electrochemical Flow Cell towards Industrial CO2 Reduction to Potassium Formate. *ChemCatChem* **2024**, *16* (4), No. e2023-00977.
(16) Gawel, A.; Jaster, T.; Siegmund, D.; Holzmann, J.; Lohmann, H.; Klemm, E.; Apfel, U.-P. Electrochemical CO2 Reduction - The Macroscopic World of Electrode Design, Reactor Concepts & Economic Aspects. *iScience* **2022**, *25* (4), 104011.
(17) Scialdone, O.; Galia, A.; Nero, G. L.; Proietto, F.; Sabatino, S.; Schiavo, B. Electrochemical Reduction of Carbon Dioxide to Formic Acid at a Tin Cathode in Divided and Undivided Cells: Effect of Carbon Dioxide Pressure and Other Operating Parameters. *Electrochim. Acta* **2016**, *199*, 332−341.
(18) Proietto, F.; Schiavo, B.; Galia, A.; Scialdone, O. Electrochemical Conversion of CO2 to HCOOH at Tin Cathode in a Pressurized Undivided Filter-Press Cell. *Electrochim. Acta* **2018**, *277*, 30−40.
(19) Ramdin, M.; Morrison, A. R. T.; de Groen, M.; van Haperen, R.; de Kler, R.; van den Broeke, L. J. P.; Trusler, J. P. M.; de Jong, W.; Vlugt, T. J. H. High Pressure Electrochemical Reduction of CO2 to Formic Acid/Formate: A Comparison between Bipolar Membranes and Cation Exchange Membranes. *Ind. Eng. Chem. Res.* **2019**, *58* (5), 1834−1847.
(20) Kudo, A.; Nakagawa, S.; Tsuneto, A.; Sakata, T. Electrochemical Reduction of High Pressure CO 2 on Ni Electrodes. *J. Electrochem. Soc.* **1993**, *140* (6), 1541.
(21) Hara, K.; Kudo, A.; Sakata, T. Electrochemical Reduction of Carbon Dioxide under High Pressure on Various Electrodes in an Aqueous Electrolyte. *J. Electroanal. Chem.* **1995**, *391* (1), 141−147.
(22) Hara, K.; Tsuneto, A.; Kudo, A.; Sakata, T. Electrochemical Reduction of CO 2 on a Cu Electrode under High Pressure: Factors That Determine the Product Selectivity. *J. Electrochem. Soc.* **1994**, *141* (8), 2097−2103.
(23) Kas, R.; Kortlever, R.; Yılmaz, H.; Koper, M. T. M.; Mul, G. Manipulating the Hydrocarbon Selectivity of Copper Nanoparticles in CO2 Electroreduction by Process Conditions. *ChemElectroChem* **2015**, *2* (3), 354−358.
(24) Wakerley, D.; Lamaison, S.; Wicks, J.; Clemens, A.; Feaster, J.; Corral, D.; Jaffer, S. A.; Sarkar, A.; Fontecave, M.; Duoss, E. B.; Baker, S.; Sargent, E. H.; Jaramillo, T. F.; Hahn, C. Gas Diffusion Electrodes, Reactor Designs and Key Metrics of Low-Temperature CO2 Electrolysers. *Nat. Energy* **2022**, *7* (2), 130−143.
(25) Jin, J.; Wicks, J.; Min, Q.; Li, J.; Hu, Y.; Ma, J.; Wang, Y.; Jiang, Z.; Xu, Y.; Lu, R.; Si, G.; Papangelakis, P.; Shakouri, M.; Xiao, Q.; Ou, P.; Wang, X.; Chen, Z.; Zhang, W.; Yu, K.; Song, J.; Jiang, X.; Qiu, P.; Lou, Y.; Wu, D.; Mao, Y.; Ozden, A.; Wang, C.; Xia, B. Y.; Hu, X.; Dravid, V. P.; Yiu, Y.-M.; Sham, T.-K.; Wang, Z.; Sinton, D.; Mai, L.; Sargent, E. H.; Pang, Y. Constrained C2 Adsorbate Orientation Enables CO-to-Acetate Electroreduction. *Nature* **2023**, *617* (7962), 724−729.
(26) Huang, L.; Gao, G.; Yang, C.; Li, X.-Y.; Miao, R. K.; Xue, Y.; Xie, K.; Ou, P.; Yavuz, C. T.; Han, Y.; Magnotti, G.; Sinton, D.; Sargent, E. H.; Lu, X. Pressure Dependence in Aqueous-Based Electrochemical CO2 Reduction. *Nat. Commun.* **2023**, *14* (1), 2958.
(27) Wei, P.; Gao, D.; Liu, T.; Li, H.; Sang, J.; Wang, C.; Cai, R.; Wang, G.; Bao, X. Coverage-Driven Selectivity Switch from Ethylene to Acetate in High-Rate CO2/CO Electrolysis. *Nat. Nanotechnol.* **2023**, *18* (3), 299−306.
(28) Wang, X.; Chen, Y.; Li, F.; Miao, R. K.; Huang, J. E.; Zhao, Z.; Li, X.-Y.; Dorakhan, R.; Chu, S.; Wu, J.; Zheng, S.; Ni, W.; Kim, D.; Park, S.; Liang, Y.; Ozden, A.; Ou, P.; Hou, Y.; Sinton, D.; Sargent, E. H. Site-Selective Protonation Enables Efficient Carbon Monoxide Electroreduction to Acetate. *Nat. Commun.* **2024**, *15* (1), 616.
(29) Xia, C.; Zhu, P.; Jiang, Q.; Pan, Y.; Liang, W.; Stavitski, E.; Alshareef, H. N.; Wang, H. Continuous Production of Pure Liquid Fuel Solutions via Electrocatalytic CO2 Reduction Using Solid-Electrolyte Devices. *Nat. Energy* **2019**, *4* (9), 776−785.
(30) Fan, L.; Xia, C.; Zhu, P.; Lu, Y.; Wang, H. Electrochemical CO2 Reduction to High-Concentration Pure Formic Acid Solutions in an All-Solid-State Reactor. *Nat. Commun.* **2020**, *11* (1), 3633.
(31) Nankya, R.; Xu, Y.; Elgazzar, A.; Zhu, P.; Wi, T.-U.; Qiu, C.; Feng, Y.; Che, F.; Wang, H. Cobalt-Doped Bismuth Nanosheet Catalyst for Enhanced Electrochemical CO2 Reduction to Electrolyte-Free Formic Acid. *Angew. Chem., Int. Ed.* **2024**, *63* (36), No. e202403671.
(32) Elgazzar, A.; Zhu, P.; Chen, F.-Y.; Hao, S.; Wi, T.-U.; Qiu, C.; Okatenko, V.; Wang, H. Electrochemical CO2 Reduction to Formic Acid with High Carbon Efficiency. *ACS Energy Lett.* **2025**, *10* (1), 450−458.
(33) Zhu, P.; Wu, Z.-Y.; Elgazzar, A.; Dong, C.; Wi, T.-U.; Chen, F.-Y.; Xia, Y.; Feng, Y.; Shakouri, M.; Kim, J. Y.; Fang, Z.; Hatton, T. A.; Wang, H. Continuous Carbon Capture in an Electrochemical Solid-Electrolyte Reactor. *Nature* **2023**, *618* (7967), 959−966.
(34) Elgazzar, A.; Wang, H. Beyond Molecular Transformations in Electrochemical Porous Solid Electrolyte Reactors. *Nat. Chem. Eng.* **2025**, *2*, 3−7.
(35) Zhang, X.; Fang, Z.; Zhu, P.; Xia, Y.; Wang, H. Electrochemical Regeneration of High-Purity CO2 from (Bi)Carbonates in a Porous Solid Electrolyte Reactor for Efficient Carbon Capture. *Nat. Energy* **2025**, *10* (1), 55−65.
(36) Kim, J. Y.; Zhu, P.; Chen, F.-Y.; Wu, Z.-Y.; Cullen, D. A.; Wang, H. Recovering Carbon Losses in CO2 Electrolysis Using a Solid Electrolyte Reactor. *Nat. Catal.* **2022**, *5* (4), 288−299.
(37) Xie, L.; Cai, Y.; Jiang, Y.; Shen, M.; Lam, J. C.-H.; Zhu, J.; Zhu, W. Direct Low Concentration CO2 Electroreduction to Multicarbon Products via Rate-Determining Step Tuning. *Nat. Commun.* **2024**, *15* (1), 10386.
(38) Zhao, Z.-H.; Huang, J.-R.; Huang, D.-S.; Zhu, H.-L.; Liao, P.-Q.; Chen, X.-M. Efficient Capture and Electroreduction of Dilute CO2 into Highly Pure and Concentrated Formic Acid Aqueous Solution. *J. Am. Chem. Soc.* **2024**, *146* (20), 14349−14356.
(39) Wang, M.; Wang, B.; Zhang, J.; Xi, S.; Ling, N.; Mi, Z.; Yang, Q.; Zhang, M.; Leow, W. R.; Zhang, J.; Lum, Y. Acidic Media Enables Oxygen-Tolerant Electrosynthesis of Multicarbon Products from Simulated Flue Gas. *Nat. Commun.* **2024**, *15* (1), 1218.
(40) Choi, B.-U.; Tan, Y. C.; Song, H.; Lee, K. B.; Oh, J. System Design Considerations for Enhancing Electroproduction of Formate from Simulated Flue Gas. *ACS Sustain. Chem. Eng.* **2021**, *9* (5), 2348−2357.
(41) Kim, B.; Seong, H.; Song, J. T.; Kwak, K.; Song, H.; Tan, Y. C.; Park, G.; Lee, D.; Oh, J. Over a 15.9% Solar-to-CO Conversion from Dilute CO2 Streams Catalyzed by Gold Nanoclusters Exhibiting a High CO2 Binding Affinity. *ACS Energy Lett.* **2020**, *5* (3), 749−757.
(42) Hou, P.; Song, W.; Wang, X.; Hu, Z.; Kang, P. Well-Defined Single-Atom Cobalt Catalyst for Electrocatalytic Flue Gas CO2 Reduction. *Small* **2020**, *16* (24), 2001896.
(43) Lin, L.; He, X.; Zhang, X.-G.; Ma, W.; Zhang, B.; Wei, D.; Xie, S.; Zhang, Q.; Yi, X.; Wang, Y. A Nanocomposite of Bismuth Clusters and Bi2O2CO3 Sheets for Highly Efficient Electrocatalytic Reduction of CO2 to Formate. *Angew. Chem., Int. Ed.* **2023**, *62* (3), No. e202214959.
(44) Zhu, P.; Xia, C.; Liu, C.-Y.; Jiang, K.; Gao, G.; Zhang, X.; Xia, Y.; Lei, Y.; Alshareef, H. N.; Senftle, T. P.; Wang, H. Direct and Continuous Generation of Pure Acetic Acid Solutions via Electrocatalytic Carbon Monoxide Reduction. *Proc. Natl. Acad. Sci. U. S. A.* **2021**, *118* (2), No. e2010868118.
(45) Wi, T.-U.; Xie, Y.; Levell, Z. H.; Feng, D.; Kim, J. Y.; Zhu, P.; Elgazzar, A.; Jeon, T. H.; Shakouri, M.; Hao, S.; Fang, Z.; Qiu, C.; Lee, H.-W.; Hicks, A.; Liu, Y.; Liu, C.; Wang, H. Upgrading Carbon Monoxide to Bioplastics via Integrated Electrochemical Reduction and Biosynthesis. *Nat. Synth.* **2024**, *3* (11), 1392−1403.
(46) Wi, T.-U.; Levell, Z. H.; Hao, S.; Elgazzar, A.; Zhu, P.; Feng, Y.; Chen, F.-Y.; Lam, W. P.; Shakouri, M.; Liu, Y.; Wang, H. Selective

https://doi.org/10.1021/acsenergylett.5c02165
ACS Energy Lett. 2025, 10, 5466−5473

and Stable Ethanol Synthesis via Electrochemical CO2 Reduction in a Solid Electrolyte Reactor. *ACS Energy Lett.* **2025**, *10* (2), 822−829.
(47) Wang, S.; Kou, T.; Baker, S. E.; Duoss, E. B.; Li, Y. Recent Progress in Electrochemical Reduction of CO2 by Oxide-Derived Copper Catalysts. *Mater. Today Nano* **2020**, *12*, 100096.
(48) Cherniack, L. H.; Hansen, K. U.; Li, Z.; Taylor, A. K.; Neyerlin, K. C.; Jiao, F. An Interfacial Engineering Approach toward Operation of a Porous Solid Electrolyte CO2 Electrolyzer. *ACS Energy Lett.* **2025**, *10* (3), 1508−1516.
(49) Fang, Z.; Zhu, P.; Zhang, X.; Feng, Y.; Wang, H. Self-Looped Electrochemical Recycling of Lithium-Ion Battery Cathode Materials to Manufacturing Feedstocks. *Nat. Chem. Eng.* **2025**, *2* (2), 142−151.

https://doi.org/10.1021/acsenergylett.5c02165
ACS Energy Lett. 2025, 10, 5466−5473